International Journal of Engineering Science 168 (2021) 103562

Contents lists available at ScienceDirect

International Journal of Engineering Science

journal homepage: www.elsevier.com/locate/ijengsci

Discrete transformation elasticity: An approach to design lattice-based polar metamaterials

Yangyang Chen, Hussein Nassar, Guoliang Huang *

Department of Mechanical and Aerospace Engineering, University of Missouri, Columbia, MO, 65211, USA

ARTICLE INFO

Keywords:
Transformation Elasticity
Discrete Elasticity
Lattice Design
Polar Metamaterials
Elastic Cloaks

ABSTRACT

The transformation method is a powerful tool providing the constitutive parameters necessary for arbitrary geometric transformations of solution fields. These constitutive parameters, in elasticity, describe a constitutive law that, unlike conventional Hooke's law, is polar and chiral and that no known solids exhibit. This raises the question of whether polar and chiral elastic solids can be designed from the bottom up as architected lattice-based materials; this design task is a major challenge in the field of transformation elasticity. The present study aims to provide a theoretically justified design methodology based on a discrete transformation method. The key idea is to let the gradient of the geometric transformation operate not only on the elastic properties but on the underlying lattice-based architecture of the solids. As an outstanding application, we leverage the proposed design paradigm to construct a polar lattice metamaterial subsequently used for elastic carpet cloaking purposes. Numerical simulations are carried to show excellent cloaking performance under different static and dynamic mechanical loads and thus demonstrate the validity of the proposed designs. The approach presented herein could promote and accelerate new designs of lattice topologies for transformation elasticity in particular and can be extended to realize other emergent elastic properties and to unlock peculiar field-warping functions other than cloaking in static and dynamic contexts.

Introduction

The theory of composites, broadly defined, continues to inform design procedures for artificial materials Milton (2002). An important thematic problem in that context is how to design materials with target elastic properties out of a limited number of elastic phases, with specific volume fractions, and using certain fabrication processes, e.g., mixing, layering, or 3D printing. The advent of metamaterials has presented the theory of composites with new challenges where the target properties are unusual in the sense that they break certain conventional symmetries of the constitutive law, e.g., the minor symmetries of Hooke's law (Kadic, Milton, van Hecke & Wegener, 2019, Frenzel, Kadic & Wegener, 2017, Liu, Huang & Hu, 2012, Lakes & Benedict, 1982, Fernandez-Corbaton et al., 2019). Most relevant to our purposes is the way in which such properties arise in the context of the transformation method where they allow to space-warp solution fields. In transformation acoustics, for instance, the design of acoustic "invisible" cloaks naturally calls for the use of "anisotropic fluids", i.e., acoustic media where stress is not necessarily hydrostatic (Norris, 2008, Cummer & Schurig, 2007, Chen et al., 2017). Remarkably, anisotropic fluids can be 3D printed out of a single solid phase in a lattice form. In that case, anisotropic fluids are better known as "pentamode materials" (Chen et al., 2017, Chen, Liu & Hu, 2015, Gokhale, Cipolla & Norris, 2012, Norris,

* Corresponding author.
E-mail address: huangg@missouri.edu (G. Huang).

https://doi.org/10.1016/j.ijengsci.2021.103562
Received 3 March 2021; Received in revised form 5 August 2021; Accepted 8 August 2021
Available online 16 August 2021
0020-7225/© 2021 Elsevier Ltd. All rights reserved.

2015). In transformation elasticity on the other hand, anisotropy is not enough, and a general space-warping transformation, namely a curvilinear change of coordinates, modifies Hooke's law into a different nonstandard constitutive law (Norris & Shuvalov, 2011). The specific form of the modified law depends on the "gauge" adopted in the change of coordinates. In the Milton-Brian-Willis gauge, the modified law is of the Willis type: it exhibits symmetric stresses but couples stresses to velocities (Norris & Shuvalov, 2011, Milton, Briane & Willis, 2006, Nassar, He & Auffray, 2015). On the other hand, in the Brun–Guenneau–Movchan gauge, the law exhibits a nonstandard elasticity tensor $\mathbf{c}$ with polar (i.e., lacking minor symmetry $c_{ijkl} \neq c_{jikl}$) and, in some cases, chiral (i.e., lacking mirror symmetry) components (Norris & Shuvalov, 2011, Brun, Guenneau & Movchan, 2009, Nassar, Chen & Huang, 2018, Nassar, Chen & Huang, 2019, Zhang, Chen, Liu & Hu, 2020, Nassar, Chen & Huang, 2020, Xu et al., 2020). This observation begs the question of how to design elastic lattice metamaterials with targeted anisotropic, polar, and chiral elasticity tensors. In this paper, we answer that question for a wide range of materials in two space dimensions.

Lattice metamaterials, including pentamodes and the kind of architected materials of interest here, are a class of artificial cellular materials made out of interconnected beam elements organized at different scales to precisely tailor material properties. Evidently, lattice materials have applications that extend beyond the realm of cloaking; in particular, they provide designs for lightweight structures (Schaedler & Carter, 2016, Surjadi et al., 2019), bone replacements (Arabnejad et al., 2016, Heinl et al., 2008), energy absorbers (Xiong et al., 2015, Hammetter, Rinaldi & Zok, 2013, Ozdemir et al., 2016), nanomaterials with ultrahigh strength, damage tolerance, and stiffness (Bauer et al., 2017, Pham, Liu, Todd & Lertthanasarn, 2019), and of other multifunctional materials (Maloney et al., 2012, Saleh, Li, Park & Panat, 2018, Jiang et al., 2018, Sun et al., 2019). Lattice metamaterials are, in a sense, universal for the realization of extreme and unusual properties. As a matter of fact, pentamodes have been originally introduced by Milton and Cherkaev as a way to prove that any elasticity tensor can be realized with an appropriate mixture of lattice materials (Milton & Cherkaev, 1995). In general, such mixtures are highly intricate and involve several interpenetrating lattices making them impractical. In some cases, however, a single lattice suffices to achieve the desired properties; such is the case of pentamodes in transformation acoustics. Here, we investigate how transformed elastic materials can be fashioned out of single-lattice metamaterials and propose a rational approach for their inverse design starting from the desired properties and resulting in 3D-printable architectures.

The desired elasticity tensors $\mathbf{c}$ in transformation elasticity are function of two parameters: (i) the elasticity tensor $\mathbf{C}$ of a standard reference medium, i.e., before applying any geometric transformations; and, (ii) the gradient $\mathbf{F}$ of a space-warping transformation ϕ which maps the reference medium to a physical space (Norris & Shuvalov, 2011). In a recent breakthrough, elastic cloaks have been designed by developing polar elastic lattices convenient for two particular classes of transformations, (*i*) that of conformal transformations ϕ where $\boldsymbol{F}$ is shear-free (i.e., proportional to a rotation) (Nassar, Chen & Huang, 2019, Nassar, Chen & Huang, 2020); and (*ii*) that of radially symmetric ϕ where $\boldsymbol{F}$ is rotation-free (Nassar, Chen & Huang, 2018, Zhang, Chen, Liu & Hu, 2020, Xu et al., 2020). By contrast, the present design paradigm holds for arbitrary transformation gradients $\boldsymbol{F}$ combining nonuniform stretch, shear, and rotation and permits to realize anisotropic materials with polar and chiral properties. The key idea is to let $\boldsymbol{F}$ operate, not only on the elastic properties to change them from $\mathbf{C}$ to $\mathbf{c}$, but on the underlying architectures themselves as well. In other words, instead of looking for architectures with the unusual tensor $\mathbf{c}$, we first target the architectures of the background medium with the conventional tensor $\mathbf{C}$. The found architectures are then transformed by $\mathbf{F}$ into a lattice material which automatically exhibits the sought-after tensor $\mathbf{c}$. The transformation rules according to which $\boldsymbol{F}$ operates on a lattice material to generate another lattice material constitute what we refer to as "*Discrete Transformation Elasticity*". A theoretical treatment of discrete transformation elasticity was first proposed by Guevara Vasquez et al. but did not lead to feasible designs (Vasquez, Milton, Onofrei & Seppecher, 2013); another relevant contribution, is the one by Bückmann et al. (Bückmann, Kadic, Schittny & Wegener, 2015), where direct lattice transformations have been suggested but ignored the polar character of the required tensors. Here, we complete these efforts in the framework of polar elasticity and propose feasible designs based on rigorous derivations taking into account the full tensorial character of the equations of elasticity that can be anisotropic, polar, and chiral simultaneously. As an outstanding application, we leverage the proposed design paradigm to construct a polar lattice metamaterial for the observation of elastic carpet cloaking. Numerical simulations are then conducted and show excellent

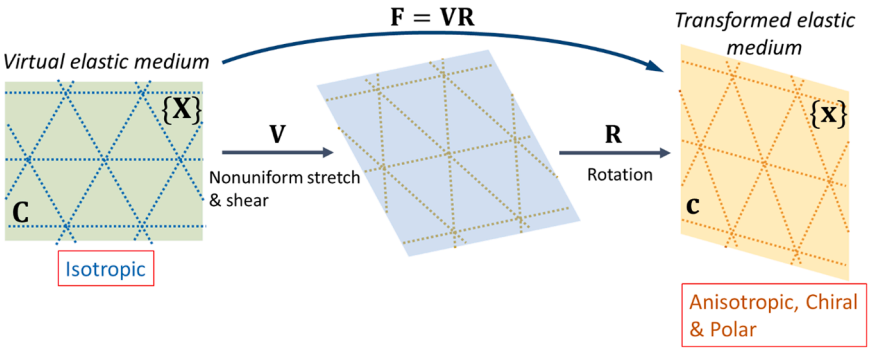

Fig. 1. Schematic representation of continuum transformation elasticity. A continuum elastic medium with the elastic tensor $\mathbf{C}$ occupies the virtual space $\{\mathbf{X}\}$. A transformed elastic medium with the elastic tensor $\mathbf{c}$ occupies the physical space $\{\mathbf{x}\}$. The transformation gradient $\mathbf{F}$ comprises nonuniform stretch, shear, and rotation. When the virtual elastic medium is isotropic, the resulted transformed elastic medium is anisotropic, chiral, and polar.

cloaking performance under shear and pressure, static and dynamic loads.

Continuum and discrete transformation elasticity

Consider a general mapping $\mathbf{x} = \phi(\mathbf{X})$ that transforms a virtual (original) domain $\{\mathbf{X}\}$ into a physical (transformed) domain $\{\mathbf{x}\}$ (see Fig. 1). The transformation ϕ can encompass any combinations of stretch, shear, and rotation. Thus, the transformation gradient $\boldsymbol{F}$ will generally decompose into $\boldsymbol{F} = \boldsymbol{VR}$ where $\boldsymbol{R}$ is orthogonal (rotation tensor) and $\boldsymbol{V}$ is symmetric positive definite (stretch tensor), as shown in Fig. 1. The virtual and physical domains are occupied by elastic media which, under an external load, are displaced by fields $\mathbf{U}(\mathbf{X})$ and $\mathbf{u}(\mathbf{x})$, respectively. We are interested in determining the constitutive properties of $\{\mathbf{x}\}$, or even its microstructure, that let the displacement field be warped according to the same transformation ϕ, that is, $\mathbf{U}(\mathbf{X}) = \mathbf{u}(\mathbf{x}) = \mathbf{u}(\phi(\mathbf{X}))$. To do so, it is particularly insightful to interpret the fields $\mathbf{u}(\mathbf{x})$ and $\mathbf{U}(\mathbf{X})$ as two different, but equivalent, sets of generalized Lagrangian coordinates, namely such that

$$\int_{\{\mathbf{X}\}} L(\nabla\mathbf{U})\mathrm{d}\mathbf{X} = \int_{\{\mathbf{x}\}} \ell(\nabla\mathbf{u})\mathrm{d}\mathbf{x} \tag{1}$$

where L and ℓ are the strain energy densities over $\{\mathbf{X}\}$ and $\{\mathbf{x}\}$, respectively. The change of coordinates formula, together with the chain rule, then yields $\ell(\nabla\mathbf{u}) = L(\nabla\mathbf{u}\mathbf{F})/J$ with $\mathbf{F} = \mathrm{d}\mathbf{x}/\mathrm{d}\mathbf{X}$ and $J = \det\mathbf{F}$ being the transformation gradient and its determinant. Note that Eq. (1) is valid for any sets of coordinate transformations $\{\mathbf{X}\} \to \{\mathbf{x}\}$. Accordingly, it is possible to warp the displacement field from $\mathbf{U}(\mathbf{X})$ to $\mathbf{u}(\mathbf{x})$ as long as $\{\mathbf{x}\}$ is composed of materials with the prescribed strain energy ℓ. In terms of the constitutive properties, when the original domain $\{\mathbf{X}\}$ has an elasticity tensor $\mathbf{C}$, the transformed domain $\{\mathbf{x}\}$ has an elasticity tensor $\mathbf{c}$ with $c_{ijkl} = F_{jm}F_{ln}C_{imkn}/J$. A close inspection of the foregoing relation shows that the transformed elasticity tensor $\mathbf{c}$ is unconventional in at least three regards: (*i*) it is polar in the sense that it lacks the minor symmetry; (*ii*) it is degenerate in the sense that it admits a number of zero modes; (*iii*) it is chiral in the sense that it lacks mirror symmetry (in 2D). Materials with such unusual properties are unavailable and lattice-based designs, in few particular cases, have only recently been found (Nassar, Chen & Huang, 2018, Nassar, Chen & Huang, 2019, Zhang, Chen, Liu & Hu, 2020, Nassar, Chen & Huang, 2020, Xu et al., 2020). This state of affairs has significantly impeded progress in transformation elasticity in comparison to its optics or acoustics counterpart.

Here, we solve the material design problem by fully embracing a discrete lattice-based transformation (see Fig. 2). Thus, we discretize L and ℓ as if they represented the strain energy densities of two lattices. We suppose then that the background medium is made out of a periodic lattice, or at least that it has the same elasticity tensor as such a lattice. The lattice is made of a set of massless springs connecting mass nodes (Fig. 2). Hence, we let

$$L(\nabla\mathbf{U}) = (1/2)\sum_{m,n,p} K^p \left\langle \nabla\mathbf{U}\left(\mathbf{X}^p_{m,n} - \mathbf{X}_{m,n}\right), \mathbf{S}^p \right\rangle^2 \Big/ A_0 \tag{2}$$

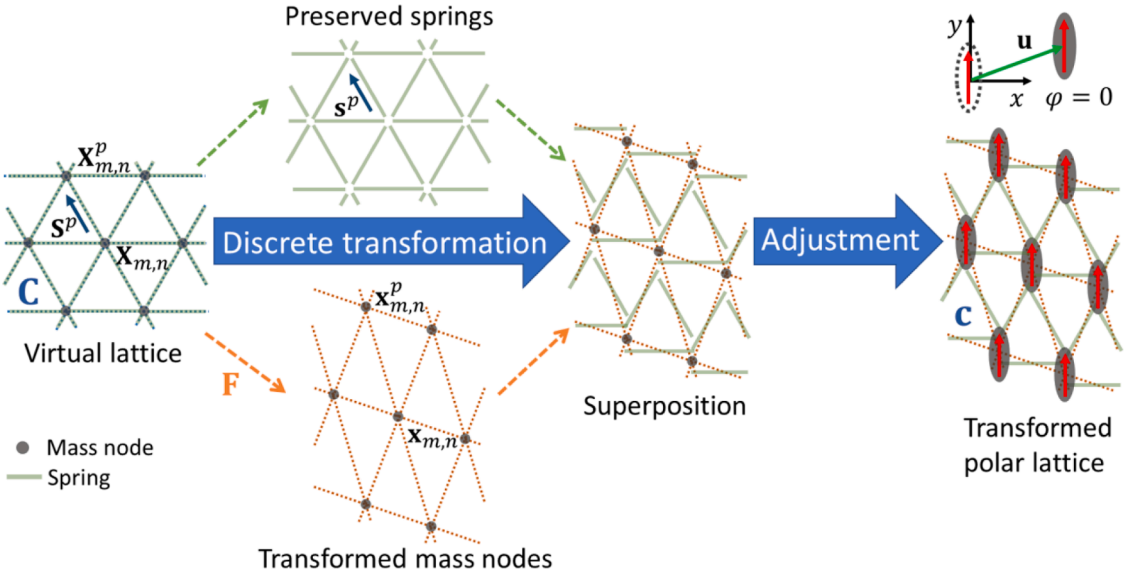

Fig. 2. Schematic representation of discrete transformation elasticity. A virtual lattice with springs connected to mass nodes is characterized by effective modulus $\mathbf{C}$. During the discrete transformation, mass nodes are transformed to new locations following $\mathbf{F}$, while springs maintains their original directions. The transformed lattice is initially misaligned and does not contact. The final transformed polar lattice is constructed by adjusting masses and springs to ensure contact and, at the same time, suppressing rotations of the masses.

be the strain energy per unit cell area A_0 of a set of springs (index p) of constants K_p and of direction $\mathbf{S}^p = \frac{\mathbf{X}^p_{m,n} - \mathbf{X}_{m,n}}{\|\mathbf{X}^p_{m,n} - \mathbf{X}_{m,n}\|}$ connecting node $\mathbf{X}_{m,n}$ of a given unit cell (index m,n) to its neighboring nodes $\mathbf{X}^p_{m,n}$. Then, per the above identity relating L and $\mathscr{E}$, domain $\{\mathbf{x}\}$ will have the same behavior as a lattice whose strain energy is

$$\mathscr{E}(\nabla\mathbf{u}) = \left(\frac{1}{2}\right)\sum_{m,n,p} k^p \left\langle \nabla\mathbf{u}\left(\mathbf{x}^p_{m,n} - \mathbf{x}_{m,n}\right), \mathbf{s}^p \right\rangle^2 \Big/ a_0, \tag{3}$$

with $(\mathbf{x}^p_{m,n} - \mathbf{x}_{m,n}) = \mathbf{F}(\mathbf{X}^p_{m,n} - \mathbf{X}_{m,n})$, $a_0 = A_0 J$, $k^p = K^p$ and $\mathbf{s}^p = \mathbf{S}^p$. In other words, the lattice of $\{\mathbf{x}\}$ can be easily deduced from that of $\{\mathbf{X}\}$ by (*i*) applying the transformation gradient $\mathbf{F}$ to the nodes of the lattice (Fig. 2) while (*ii*) leaving the springs constants and directions, as they were (Fig. 2). In particular, note that the lattice vectors anchored at the nodes, such as $\mathbf{X}^p_{m,n} - \mathbf{X}_{m,n}$, and the spring orientation $\mathbf{S}^p$ do not transform in the same fashion; indeed, $\mathbf{s}^p \neq \frac{\mathbf{x}^p_{m,n} - \mathbf{x}_{m,n}}{\|\mathbf{x}^p_{m,n} - \mathbf{x}_{m,n}\|}$. Last, to maintain physical contact between the mass nodes and the misaligned springs, the mass nodes must assume a finite size and become rigid bodies (see the transformed polar lattice in Fig. 2). This has the unintended effect of introducing an extra rotational degree of freedom which must be suppressed using an external ground or other rotational resonant substructures (Nassar, Chen & Huang, 2018, Nassar, Chen & Huang, 2019, Zhang, Chen, Liu & Hu, 2020, Nassar, Chen & Huang, 2020, Xu et al., 2020). Together, the misalignment and the suppressed rotations, are responsible for the unconventional properties of the transformed tensor $\mathbf{c}$. It is also important here to stress that the original domain $\{\mathbf{X}\}$ need not be a lattice, and only to behave like one. In particular, all isotropic materials with a Poisson's coefficient equal to 1/3 behave like a triangular truss and can therefore be transformed in this fashion. More generally, square, rectangular, and oblique lattices with anisotropic effective tensors $\mathbf{C}$ can be transformed in the same manner. Conversely, the availability of a lattice representation of the original domain is the only limitation weighing on the present approach.

Given that the behavior post-transformation exhibits asymmetric stresses, it would be tempting to describe it in the general context of micropolar elasticity (Pasternak & Dyskin, 2018). This would be uncalled however for two main reasons: on one hand, the original medium is a classical (Cauchy) continuum and therefore should transfer no couple stresses to the cloaked domain. On the other hand, the extra degrees of freedom of a micropolar medium, namely microrotations, do not appear in the strain energy density $\mathscr{E}$. Accordingly, the transformed domain remains of Cauchy type, with a single stress measure, albeit an asymmetric one, and a single, again asymmetric, strain measure. The asymmetry can be explained by recalling Cauchy's second law of motion, $\sigma_{ij} - \sigma_{ji} = e_{ijk}c_k$, namely that skew stresses are acceptable as long as they are in balance with an appropriate torque density. This torque density is

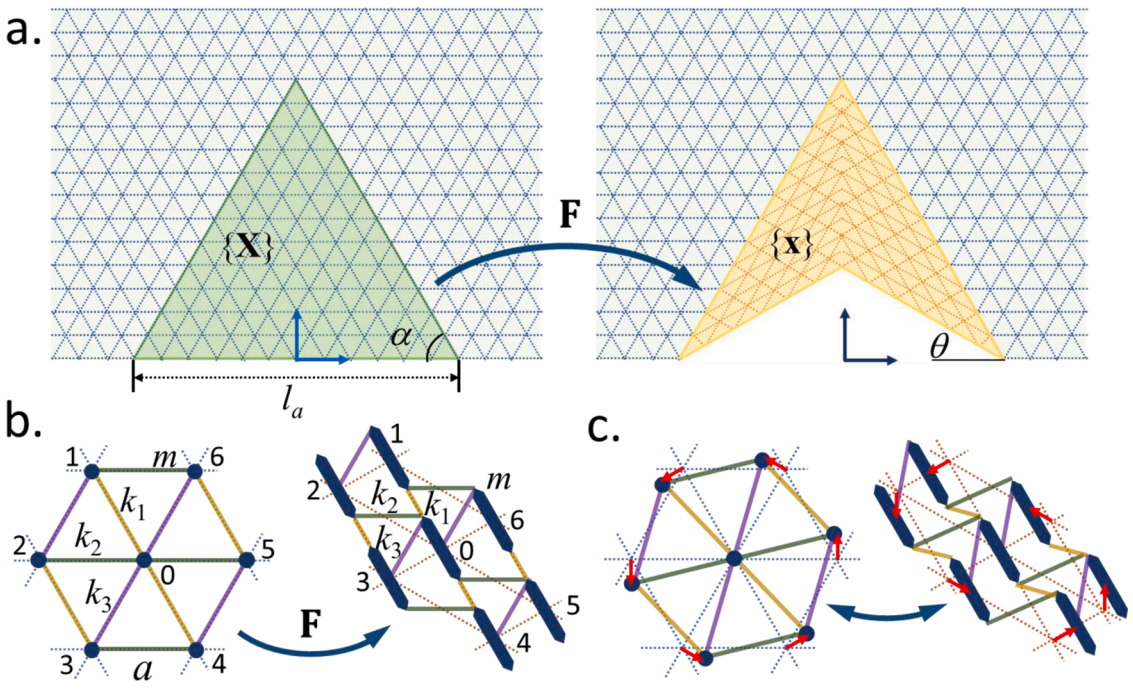

Fig. 3. Design of the discrete mass-spring polar lattice for a carpet cloak. (a) Geometric transformation for realizing a carpet cloak concealing a triangular void; (b) The mass-spring lattice is designed using the discrete transformation. For the design, $\alpha = 60°$, and the lengths of springs, k_1, k_2, k_3, and the rigid masses are $a\left[1 - \frac{2\sqrt{3}}{3}\tan(\theta)\right]$, $a\left[1 - \frac{\sqrt{3}}{3}\tan(\theta)\right]$, $a\left[1 - \frac{\sqrt{3}}{3}\tan(\theta)\right]$, and $\frac{2\sqrt{3}a}{3}\tan(\theta)$, respectively; (c) Zero-mode of the transformed lattice is equivalent to the rigid rotation of the virtual lattice.

exactly what impedes mass rotation in our designs. Simply, rather than them being constant, the torques are proportional to the applied strain. Cauchy elasticity augmented with torques that are proportional to strain constitutes what we refer to as "*polar elasticity*" (Nassar, Chen & Huang, 2018, Nassar, Chen & Huang, 2019). It is when the original medium itself is micropolar that one needs to consider how micro-rotations and couple-stresses transform, but such a generalization is out of the scope of the present paper.

A polar lattice for elastic carpet cloaking

Having introduced the continuous and discrete versions of transformation elasticity, it is time to illustrate the usefulness of the suggested paradigm in the design of polar lattices displaying nonstandard elastic properties never realized before. Our particular interest is in constructing an elastic carpet cloak with material properties that are uniform in space; this can be very advantageous from a manufacturing point of view. With that in mind, we apply a geometric transformation that linearly compresses a triangular domain in the virtual space (shaded green area) into a concave polygon in the physical domain (shaded yellow area). The transformation leaves a void along the lower boundary where an object can be concealed; the other boundaries remain unchanged (see Fig. 3a). Formally, the transformation ϕ reads

$$x = X, \quad y = \frac{\tan(\alpha) - \tan(\theta)}{\tan(\alpha)} Y + [l_a - \mathrm{sgn}(x)x]\tan(\theta), \tag{4}$$

where α, θ and l_a are two angles and a length characterizing the triangular domain and void pre- and post-transformation and are shown in Fig. 3a. We then obtain the deformation gradient of ϕ as

$$\mathbf{F} = \begin{bmatrix} 1 & 0 \\ -\mathrm{sgn}(x)\tan(\theta) & 1 - \dfrac{\tan(\theta)}{\tan(\alpha)} \end{bmatrix} \tag{5}$$

The polar decomposition leads to

$$\mathbf{V} = \begin{bmatrix} p_1\cos^2(\varphi) + p_2\sin^2(\varphi) & (p_2 - p_1)\cos(\varphi)\sin(\varphi) \\ (p_2 - p_1)\cos(\varphi)\sin(\varphi) & p_2\cos^2(\varphi) - p_1\sin^2(\varphi) \end{bmatrix}, \ \mathbf{R} = \mathbf{V}^{-1}\mathbf{F} \tag{6}$$

where $p_{1,2} = \frac{1+F_{21}^2+F_{22}^2}{2} \mp \sqrt{\left(\frac{1-F_{21}^2-F_{22}^2}{2}\right)^2 + F_{21}^2}$ and $\tan(-2\varphi) = \frac{2F_{21}}{1-F_{21}^2-F_{22}^2}$. It can be clearly seen that the stretch is non-isotropic, as $V_{11} \neq V_{22}$. In addition, the transformation comprises a shear deformation, since $V_{12} = V_{21} \neq 0$. Finally, the deformed grid needs to experience a rigid rotation $\mathbf{R} \neq \mathbf{I}$ to realize the transformation gradient **F**.

Assume the material in the virtual space is isotropic with Lamé parameters (λ, μ) and mass density ρ_0. Applying the rules of transformation elasticity (Norris & Shuvalov, 2011), the mass density and constitutive relations of the transformed material (i.e., the cloak in our context) read

$$\rho = \rho_0 A, \tag{7}$$

$$\begin{bmatrix} \sigma_{11} \\ \sigma_{22} \\ \sigma_{12} \\ \sigma_{21} \end{bmatrix} = \begin{bmatrix} (\lambda+2\mu)A & \lambda & (\lambda+2\mu)C & 0 \\ \lambda & (\lambda+2\mu)/A + \mu BC & (\lambda+\mu)B & \mu c \\ (\lambda+2\mu)C & (\lambda+\mu)B & \mu/A + (\lambda+2\mu)BC & \mu \\ 0 & \mu C & \mu & \mu A \end{bmatrix} \begin{bmatrix} e_{11} \\ e_{22} \\ e_{12} \\ e_{21} \end{bmatrix}, \tag{8}$$

with $A = \frac{\tan(\alpha)}{\tan(\alpha)-\tan(\theta)}$, $B = -\mathrm{sgn}(x)\tan(\theta)$ and $C = AB$. Eq. (7) indicates that the total mass of an area in the virtual space is equal to the total mass of its transformed area in the physical space. As for the matrix in the right-hand side of Eq. (8), it represents the transformed elastic tensor **c**. Therein, note how the properties of cloak should be anisotropic, as $c_{1111} \neq c_{2222}$ and $c_{1212} \neq c_{2121}$ due to the anisotropic stretch in the transformation. Furthermore, the transformed material needs to be chiral ($c_{1211} \neq c_{2111}$ and $c_{1222} \neq c_{2122}$), and the material is not mirror symmetric since the transformation comprises a rotation. If we are able to design a "cloaking material", i.e., a medium equivalent to the transformed material, described in Eqs. (7) and (8), then we are able to demonstrate a cloaking behavior for elastic waves in the physical space.

We tackle the inverse problem of designing the cloaking material using discrete transformation elasticity. Hereafter, we specify Eq. (8) to the case a reference medium with a Poisson's ratio of 1/3 ($\lambda = \mu$). Such a medium is conveniently represented by a triangular lattice with massless springs connecting massive nodes (see Fig. 3b; left panel). The length of the springs is denoted by a. The spring constants (k_1, k_2, k_3) and mass m of the nodes can be determined from the isotropic material properties by $k_1 = k_2 = k_3 = \frac{4\mu}{\sqrt{3}}$ and $m = \frac{\sqrt{3}\rho_0 a^2}{2}$. Performing the proposed discrete transformation, mass nodes of the virtual lattice are mapped to new locations in the transformed space following the transformation ϕ (see Points 0–6 in Fig. 3b before and after the transformation), and directions of the connecting springs remain as they were in the virtual lattice. To make masses and springs physically connected, we adjust the lengths of the springs (keeping their constants unchanged) as well as the sizes of the rigid masses (keeping their masses unchanged); the specific shape of the rigid masses is irrelevant. While the lattice configuration can be arbitrary in principle, avoiding overlap among

masses and springs will lead to simpler and more practical designs. In the adopted design, we selected elongated hexagonal rigid masses, and enforce springs k_1 and k_2 to the locations that transformed from ϕ. We first connect the rigid masses on Points 0 and 1 with the spring k_1 (see the right figure in Fig. 3b). By doing so, rigid masses must be in alignment with the spring k_1 to ensure periodicity. We then connect the rigid masses on Points 0 and 2 with the spring k_2 (see the right figure in Fig. 3b). Lengths of springs and masses are consequently determined after this procedure. Finally, the spring k_3 is adjusted into the transformed lattice by connecting Point 0 to the rigid mass on Point 6. In the design, all contacts are assumed to be hinge-like, and rotations of masses are suppressed.

Now we focus on the homogenized elastic response of the transformed lattice. Our aim is to validate the design step. Using the volume average approach (Nassar, Chen & Huang, 2018), the effective elastic constants of the transformed spring-mass system can be analytically obtained in terms of θ, k_1, k_2, and k_3 for $x > 0$ as (See Supplementary Information for details)

$$\begin{aligned}
&\bar{c}_{1111} = \overline{A}(16k_1 + k_2 + k_3),\ \bar{c}_{1122} = \overline{A}\left(3k_2 + \overline{B}k_3\right),\ \bar{c}_{1112} = \overline{A}\left(-16\tan(\theta)k_1 - \sqrt{3}k_2 + \overline{C}k_3\right),\\
&\bar{c}_{1121} = \sqrt{3}\overline{A}(-k_2 + k_3),\ \bar{c}_{2222} = \overline{A}\left(9k_2 + 3\overline{C}^2k_3\right),\ \bar{c}_{2212} = \sqrt{3}\overline{A}\left(-3k_2 + \overline{C}^2k_3\right),\\
&\bar{c}_{2221} = 3\overline{A}\left(-\sqrt{3}k_2 + \overline{C}k_3\right),\ \bar{c}_{1212} = \overline{A}\left(16\tan^2(\theta)k_1 + 3k_2 + \overline{C}^2k_3\right),\ \bar{c}_{1221} = \overline{A}\left(3k_2 + \overline{B}k_3\right),\\
&\bar{c}_{2121} = 3\overline{A}(k_2 + k_3),
\end{aligned} \tag{9}$$

where $\overline{A} = \frac{1}{8[\sqrt{3}-\tan(\theta)]}$, $\overline{B} = 3 - 2\sqrt{3}\tan(\theta)$ and $\overline{C} = \sqrt{3} - 2\tan(\theta)$. Letting the spring constants be those of the virtual lattice: $k_1 = k_2 = k_3 = \frac{4\mu}{\sqrt{3}}$ and $\lambda = \mu$, the obtained effective elastic moduli in Eq. (9) are exactly those that appear in the transformed material parameters of Eq. (8); thus our predictions based on discrete transformation elasticity are valid.

It should be worth mentioning that the lattice we constructed through discrete transformation elasticity naturally admits a zero-

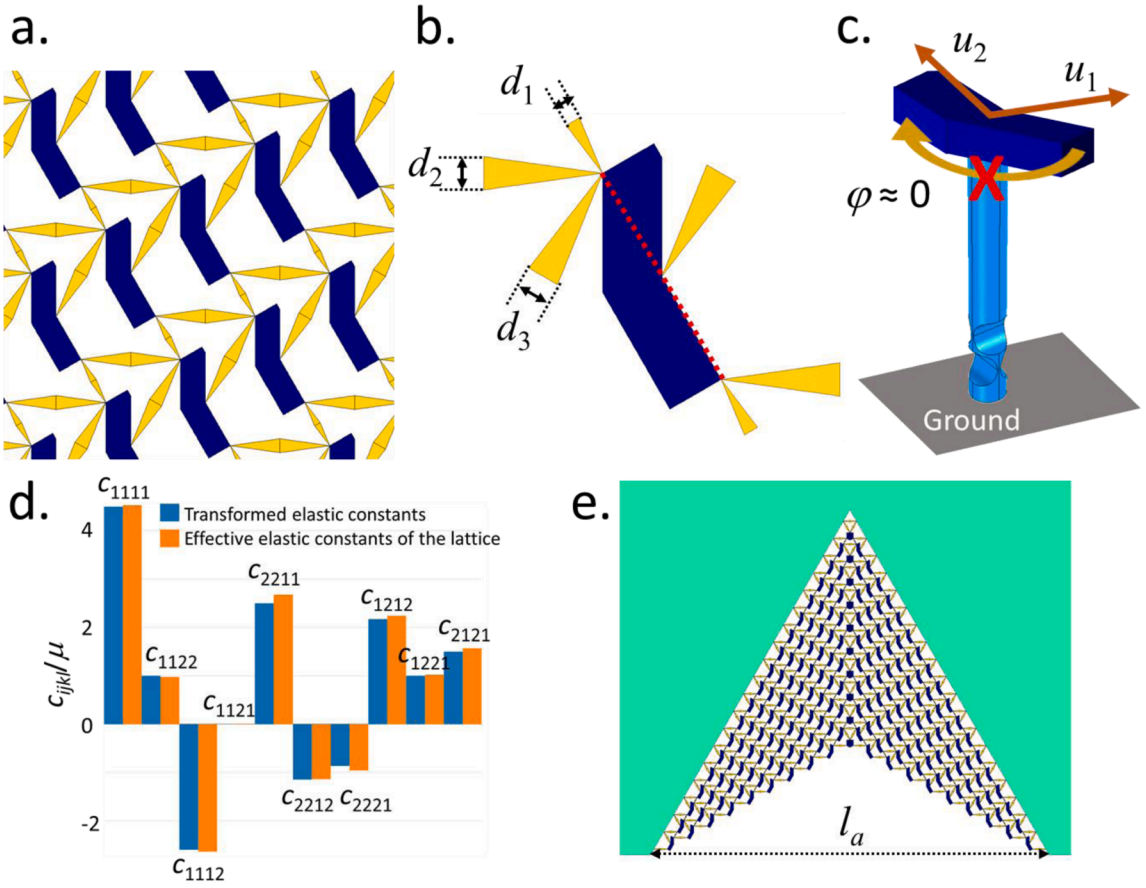

Fig. 4. Microstructure realization of the lattice-based polar metamaterial. (a) The topology of the lattice metamaterial; (b) The unit cell of the lattice metamaterial. In the design, $a = 18$ mm, $\theta = 30^\circ$, $d_1 = 0.38$ mm, and $d_2 = d_3 = 0.84$ mm. The Young's modulus and Poison's ratio of the soft and hard materials are 1 GPa, 0.33, 100 GPa, and 0.33, respectively; (c) The hard material is connected to the ground with a rod that supports near-zero rotation but nearly free in-plane translation; (d) Effective elastic constants of the lattice metamaterial in comparison with the desired transformed elastic constants; (e) A carpet cloak is constructed using the lattice metamaterial, where $l_a = 360$ mm. For the carpet cloaking, material parameters of the background material are selected as $\lambda = \mu = 9.14$ MPa and $\rho_0 = 1000$ kg/m^3. To satisfy the mass requirement, the mass density of the hard material is assumed as $\rho_h = 7035$ kg/m^3.

mode $\mathbf{e}_0 = \mathbf{E}_0\mathbf{F}^{-1}$, where $\mathbf{E}_0 = \begin{bmatrix} 0 & 1 \\ -1 & 0 \end{bmatrix}$. Physically, the rigid rotation in the virtual lattice is transformed into a zero-mode in the transformed lattice. As shown in Fig. 3c, the motions on Points 1-6 are identical before (when the motion is a rigid rotation) and after (when the motion is a zero-mode) the transformation, and naturally satisfy the displacement gauge $\mathbf{U}(\mathbf{X}) = \mathbf{u}(\mathbf{x})$ adopted in the transformation.

Microstructure realization of the polar metamaterial

Informed by the transformed mass-spring lattice, we now explore ways to numerically design a polar metamaterial to confirm the extent to which a candidate metamaterial microstructure meets the requirements of a cloaking material and is ready to be fabricated. Figs. 4a and 4b illustrate the metamaterial design, where a hard material (blue area) is employed for constructing rigid masses, and a soft material (yellow area) functions as springs. The geometry of the hard material can be modified to meet the mass density requirement as long as it maintains contact with the soft material at the three points located on the red dotted line (See detailed geometric parameters of this design in Supplementary Information). To suppress the rotational motion of each mass, we introduce a rod connecting the mass to the ground (see Fig. 4c). The rod near the ground is indented to significantly reduce its bending stiffness along u_1 and u_2 directions. As a result, the rotational stiffness of the rod is much greater than its bending stiffness. Therefore, rotation of the supported mass is efficiently suppressed and only in-plane translation is allowed. The conventional diamond-shaped bar made of the soft material is selected to mimic the spring (Fig. 4b), which leads to negligible bending moments at its ends when the bar twists around the mass. By varying parameters d_1, d_2, and d_3, we can realize different effective spring constants $k_{eff} = k_1 = k_2 = k_3$ for the transformed lattice.

Having selected geometric and material parameters of the metamaterial, we now determine the effective elastic constants needed for the cloaking application. We numerically calculate the effective elastic constants based on the volume average approach similar to that employed analytically in (Nassar, Chen & Huang, 2018). In the approach, the mechanical response of the metamaterial and the effective medium is considered equivalent if the strain energy density of the former is equal to that of the latter. To obtain the effective $\mathbf{c}$, ten independent numerical tests are performed for solving the ten independent components in $\mathbf{c}$ dictated by the major symmetry

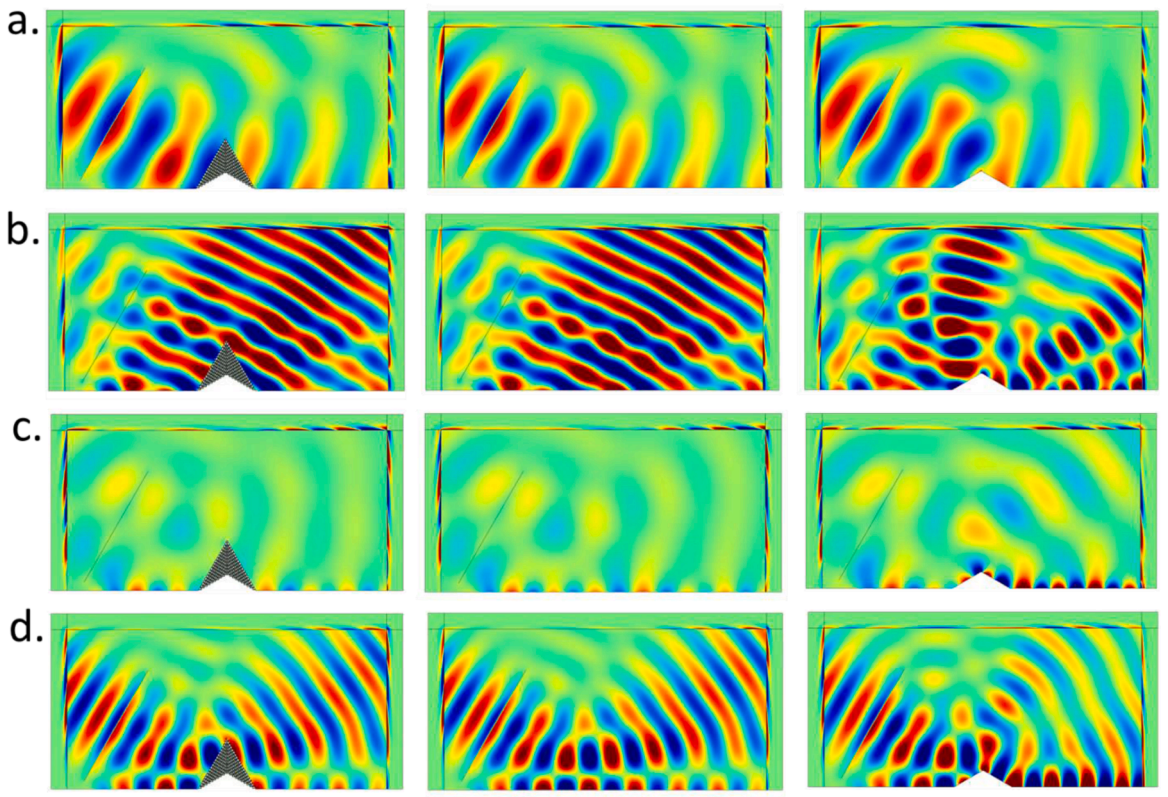

Fig. 5. Numerical simulations of the carpet cloak with the lattice-based polar metamaterial. Figures in the first column show the results when the lattice metamaterial is embedded in the background medium for cloaking. Figures in the second column show the results when the background medium is intact. Figures in the third column show the results when the void is non-coated. (a) Divergence of the displacement field with a pressure incidence; (b) Curl of the displacement field with a pressure incidence; (c) Divergence of the displacement field with a shear incidence; (d) Curl of the displacement field with a shear incidence.

($c_{ijkl} = c_{klij}$). In each of the tests, we apply the rotational constraint on the left bottom boundary of the mass to mimic the required grounded connection. We prescribe displacements on the boundaries of the unit cell to induce different strain states. Other boundaries are left free. During the simulations, we first individually apply the four uniform strain states: two uniaxial and two shear strains (e_{11}, e_{22}, e_{12}, or e_{21}), and then apply the six mixed strains: ($\{e_{11}, e_{22}\}$, $\{e_{11}, e_{12}\}$, $\{e_{11}, e_{21}\}$, $\{e_{22}, e_{12}\}$, $\{e_{22}, e_{21}\}$, or $\{e_{12}, e_{21}\}$). The strain energy per unit cell is numerically calculated for each of the ten cases with the plane stress hypothesis, from which the ten independent elastic constants can be retrieved. As shown in Fig. 4d, effective elastic constants of the lattice metamaterial (orange bars) agree very well with the transformed parameters in Eq. (8) (blue bars), which demonstrates the validity of the microstructure design.

Cloaking simulations

With the proposed microstructure of the lattice-based metamaterial, we are ready to construct a carpet cloak for elastic wave propagation tests (see Fig. 4e). Since the lattice-based metamaterial is originated from the discrete transformation elasticity, the metamaterial can automatically match the transformed physical space without any geometric alterations. This procedure, therefore, provides significant advantages in building lattice topologies for transformation elasticity. The number of unit cells in the cloak is chosen sufficiently large so as to enable satisfactory cloaking performance but not too large so as to avoid impractical simulation times. In the design, we chose 19 unit cells in the bottom row of the lattice, and tessellate them row-by-row with a total of 19 rows to create the carpet cloak. Note that the lattice metamaterial has seamless connections with the background material as shown in Fig. 4e. From a fabrication point of view, the total mass of the hard material can be tuned or adjusted by geometry modifications. In particular, special treatments are made for masses on the middle line of the cloak, where discontinuities emerge. We merge the two half masses into one mass and properly enlarge its area equal to the area of other masses.

In numerical simulations, Navier's equations in the background medium and in the lattice metamaterial are solved using COMSOL Multiphysics. Perfectly matched layers surrounding the background medium are adopted to suppress reflected waves from boundaries. Incident waves with Gaussian profiles in the direction of -60° are emitted to the cloak region (see Supplementary Information for other incident angles). Simulation results are shown in Fig. 5 for an incident pressure wave (Figs. 5a and 5b) and incident shear wave (Figs. 5c and 5d) at 400 Hz. Figures in the first column show the results when the lattice metamaterial is embedded in the background medium for cloaking. For reference, we perform the same simulations where the background medium is intact (the second column) and the void is non-coated (the third column). The divergence and curl of the displacement field are shown in Figs. 5a and 5c and Figs. 5b and 5d, respectively. It is clearly seen that the designed lattice metamaterial demonstrates excellent cloaking performance as it almost perfectly suppresses pressure, shear, and Rayleigh scattering due to the presence of the void. Specifically, the lattice metamaterial significantly reduce scattered shear waves from the void, which are more sensitive to defects compared with pressure waves, due to the shorter wavelength. Simulations are also conducted to study the cloaking performance of the lattice metamaterial under different incidence angles (See Supplementary Information). The results still demonstrate an excellent cloaking performance.

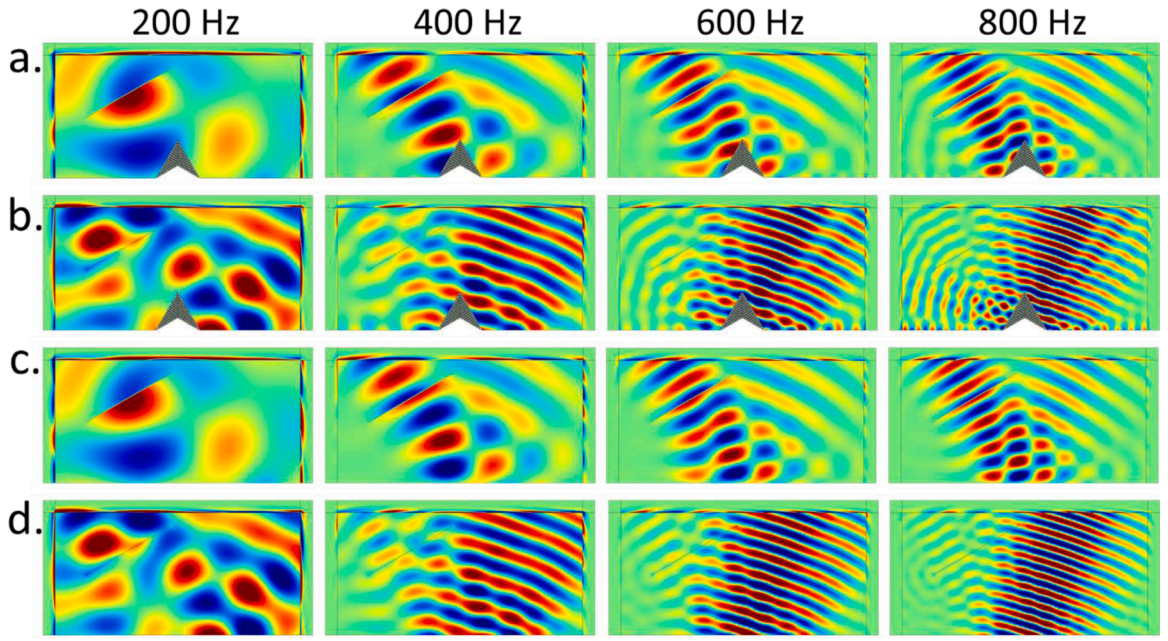

Fig. 6. Numerical simulations of the carpet cloak with -30° incidence at different frequencies. Figures in the first to fourth columns show the results at 200, 400, 600, and 800 Hz, respectively. (a,b) Divergence (a) and curl (b) of the displacement field with a pressure incidence, where the cloak is embedded in the background medium; (c,d) Divergence (c) and curl (d) of the displacement field with a pressure incidence, where the background medium is intact.

The lattice metamaterial we designed comprises no resonance structures, implying that the design could be operated at much broader frequency regions and as long as the unit cell size is small compared to the incident wavelength (that said, there are no limitations on the size of the cloaked void). To demonstrate this, we perform numerical simulations at different frequencies. As shown in Fig. 6, pressure waves are excited in the direction of -30°, and we compare the cloaking performance of the metamaterial (Figs. 6a and 6b: Divergence and curl of the displacement field) with the wave fields where the background medium is intact (Figs. 6c and 6d: Divergence and curl of the displacement field). In the figure, the first to fourth columns show the simulation results at 200, 400, 600, and 800 Hz, respectively. It can be clearly seen that good cloaking performances still retain at frequencies below 600 Hz, whereas, at 800 Hz, the shear wave field produced by the metamaterial cloak slightly deviates from that reflected from a flat boundary. To improve the performance, one needs to reduce the size of the metamaterial unit cell.

Besides dynamic pressure and shear loads, the lattice metamaterial cloak can also hide the void from static loads. In the static numerical tests, we fix the right boundary of the background plate and prescribe displacements on its left boundary. Other boundaries are left free. The prescribed displacement is along either horizontal (Figs. 7a and 7b) or vertical (Figs. 7c and 7d) directions to induce elongation or shear in the background plate. Similar to Fig. 5, the first column in Fig. 7 shows the results when the lattice metamaterial cloak is embedded, and the second and third columns are for the intact background medium and the non-coated void. Again, the divergence and curl of the displacement field are shown in Figs. 7a and 7c and Figs. 7b and 7d, respectively. We can easily find the lattice metamaterial cloak significantly improves the pressure and shear fields when the background plate undergoes elongation. In addition, the triangular void is insensitive to the shear load, where the figures in the first to third columns are nearly identical. Finally, it is also worth mentioning that the modulus of the hard material can be reduced in real designs, whereas quantitative studies should be performed to ensure the cloaking performance.

Conclusions

In conclusion, we report a simple approach based on discrete transformation elasticity to design lattice-based polar metamaterials that can automatically satisfy constitutive requirements from arbitrary coordinate transformations. In particular, we engineer a lattice metamaterial that exhibits desired polarity, chirality, and anisotropy of a transformed continuum. Based on this polar metamaterial, an elastic carpet cloak is constructed and demonstrated numerically for concealing a triangular void. The research establishes a

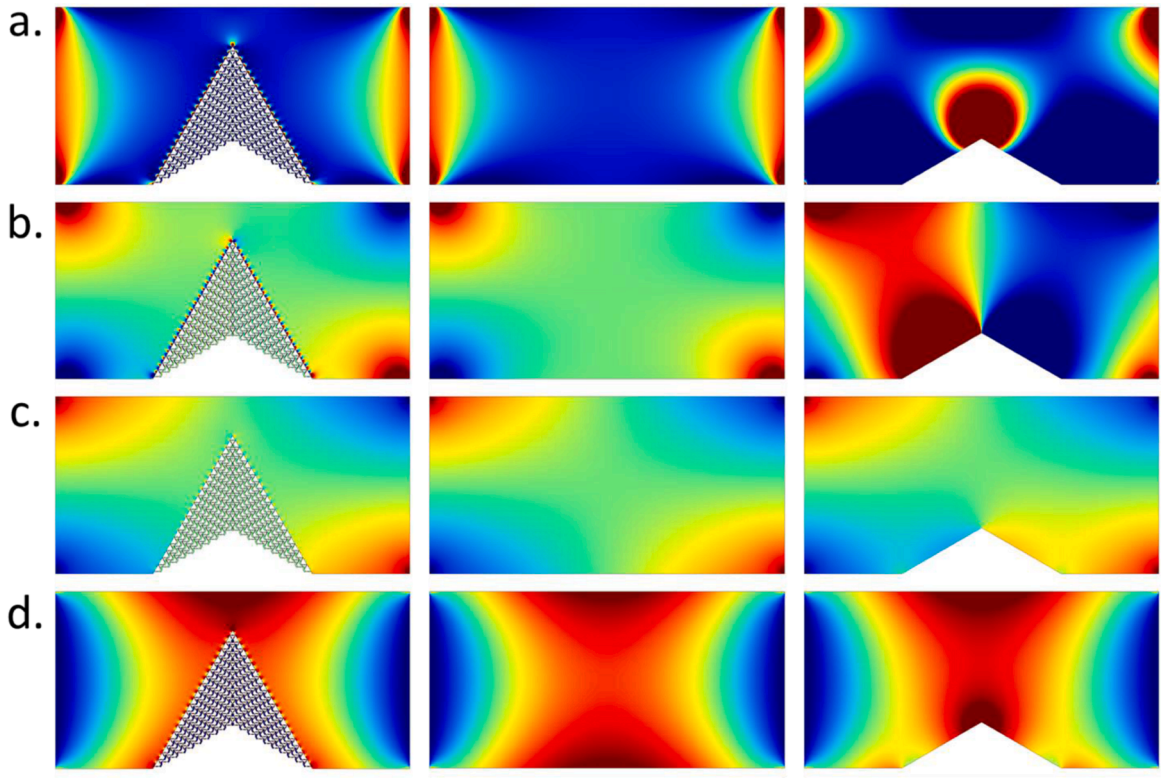

Fig. 7. Numerical simulations of the carpet cloak with static loads. Figures in the first column show the results when the lattice metamaterial is embedded in the background medium for cloaking. Figures in the second column show the results when the background medium is intact. Figures in the third column show the results when the void is non-coated. (a) Divergence of the displacement field with an elongation along the horizontal direction; (b) Curl of the displacement field with an elongation along the horizontal direction; (c) Divergence of the displacement field with a shear along the horizontal direction; (d) Curl of the displacement field with a shear along the horizontal direction.

theoretical framework for tackling the inverse design problems of lattice-based materials targeting transformed macroscopic constitutive tensors, not only for those required by elastic cloaks. Given the fact that transformation elasticity is a highly flexible method for exploiting new material parameters by varying coordinate transformations or materials in the virtual space, the lattice metamaterials designed based on discrete transformation elasticity could foster a wide range of control functions in dynamics and statics in general i.e. waveguiding, illusion, and shape morphing. Furthermore, the metamaterials designed based on this approach is ready to be used without geometric alterations or discontinuities. This approach, therefore, holds advantages over other methods in building lattice-based topologies related to transformation elasticity. As far as the proposed approach itself goes, it generalizes to 3D in a straightforward manner; the structure will simply extend in a third periodicity direction along which the geometry and the elastic properties are determined by the same principles that determined the in-plane properties. In 3D, fabrication becomes more challenging since a 3D system of grounded rods would be seriously impractical (Xu et al., 2020). In that case, the rotations could be impeded dynamically by leveraging the rotational resonance of appropriately designed embedded resonators (Nassar, Chen & Huang, 2020).

Declaration of Competing Interest

None.

Acknowledgements

The authors thank Graeme Milton for valuable discussions. This work is supported by the Army Research Office under Grant No. W911NF-18-1-0031 with Program Manager Dr. Daniel Cole.

Author contributions

Y.C. and G.H. proposed the design concept; Y.C. and H.N. performed theoretical and numerical investigations; G.H. supervised the research; All the authors discussed the results and wrote the manuscript.

Supplementary materials

Supplementary data associated with this article can be found, in the online version, at 10.1016/j.ijengsci.2021.103562.

References

Milton, G. W. (2002). *The theory of composites*. Cambridge: Cambridge University Press (ISBN 9780521781251).
Kadic, M., Milton, G. W., van Hecke, M., & Wegener, M. (2019). 3D metamaterials. *Nature Reviews Physics, 1*(3), 198–210.
Frenzel, T., Kadic, M., & Wegener, M. (2017). Three-dimensional mechanical metamaterials with a twist. *Science, 358*(6366), 1072–1074.
Liu, X. N., Huang, G. L., & Hu, G. K. (2012). Chiral effect in plane isotropic micropolar elasticity and its application to chiral lattices. *Journal of the Mechanics and Physics of Solids, 60*(11), 1907–1921.
Lakes, R. S., & Benedict, R. L. (1982). Noncentrosymmetry in micropolar elasticity. *International Journal of Engineering Science, 20*(10), 1161–1167.
Fernandez-Corbaton, I., Rockstuhl, C., Ziemke, P., Gumbsch, P., Albiez, A., Schwaiger, R., & Wegener, M. (2019). New twists of 3D chiral metamaterials. *Advanced Materials, 31*(26), Article 1807742.
Norris, A. N. (2008). Acoustic cloaking theory. *Proceedings of the Royal Society A: Mathematical, Physical and Engineering Sciences, 464*(2097), 2411–2434.
Cummer, S. A., & Schurig, D. (2007). One path to acoustic cloaking. *New Journal of Physics, 9*(3), 45.
Chen, Y., Zheng, M., Liu, X., Bi, Y., Sun, Z., Xiang, P., & Hu, G. (2017). Broadband solid cloak for underwater acoustics. *Physical Review B, 95*(18), Article 180104.
Chen, Y., Liu, X., & Hu, G. (2015). Latticed pentamode acoustic cloak. *Scientific reports, 5*(1), 1–7.
Gokhale, N. H., Cipolla, J. L., & Norris, A. N. (2012). Special transformations for pentamode acoustic cloaking. *The Journal of the Acoustical Society of America, 132*(4), 2932–2941.
Norris, A. N. (2015). Acoustic cloaking. *Acoust. Today, 11*(1), 38–46.
Norris, A. N., & Shuvalov, A. L. (2011). Elastic cloaking theory. *Wave Motion, 48*(6), 525–538.
Milton, G. W., Briane, M., & Willis, J. R. (2006). On cloaking for elasticity and physical equations with a transformation invariant form. *New Journal of Physics, 8*(10), 248.
Nassar, H., He, Q. C., & Auffray, N. (2015). Willis elastodynamic homogenization theory revisited for periodic media. *Journal of the Mechanics and Physics of Solids, 77*, 158–178.
Brun, M., Guenneau, S., & Movchan, A. B. (2009). Achieving control of in-plane elastic waves. *Applied Physics Letters, 94*(6), Article 061903.
Nassar, H., Chen, Y. Y., & Huang, G. L. (2018). A degenerate polar lattice for cloaking in full two-dimensional elastodynamics and statics. *Proceedings of the Royal Society A, 474*(2219), Article 20180523.
Nassar, H., Chen, Y. Y., & Huang, G. L. (2019). Isotropic polar solids for conformal transformation elasticity and cloaking. *Journal of the Mechanics and Physics of Solids, 129*, 229–243.
Zhang, H. K., Chen, Y., Liu, X. N., & Hu, G. K. (2020). An asymmetric elastic metamaterial model for elastic wave cloaking. *Journal of the Mechanics and Physics of Solids, 135*, Article 103796.
Nassar, H., Chen, Y. Y., & Huang, G. L. (2020). Polar metamaterials: A new outlook on resonance for cloaking applications. *Physical Review Letters, 124*(8), Article 084301.
Xu, X., Wang, C., Shou, W., Du, Z., Chen, Y., Li, B., & Huang, G. (2020). Physical realization of elastic cloaking with a polar material. *Physical Review Letters, 124*(11), Article 114301.
Schaedler, T. A., & Carter, W. B. (2016). Architected cellular materials. *Annual Review of Materials Research, 46*, 187–210.
Surjadi, J. U., Gao, L., Du, H., Li, X., Xiong, X., Fang, N. X., & Lu, Y. (2019). Mechanical metamaterials and their engineering applications. *Advanced Engineering Materials, 21*(3), Article 1800864.

Arabnejad, S., Johnston, R. B., Pura, J. A., Singh, B., Tanzer, M., & Pasini, D. (2016). High-strength porous biomaterials for bone replacement: A strategy to assess the interplay between cell morphology, mechanical properties, bone ingrowth and manufacturing constraints. *Acta biomaterialia, 30*, 345–356.

Heinl, P., Müller, L., Körner, C., Singer, R. F., & Müller, F. A. (2008). Cellular Ti–6Al–4V structures with interconnected macro porosity for bone implants fabricated by selective electron beam melting. *Acta biomaterialia, 4*(5), 1536–1544.

Xiong, J., Mines, R., Ghosh, R., Vaziri, A., Ma, L., Ohrndorf, A., & Wu, L. (2015). Advanced micro-lattice materials. *Advanced Engineering Materials, 17*(9), 1253–1264.

Hammetter, C. I., Rinaldi, R. G., & Zok, F. W. (2013). Pyramidal lattice structures for high strength and energy absorption. *Journal of Applied Mechanics, 80*(4).

Ozdemir, Z., Hernandez-Nava, E., Tyas, A., Warren, J. A., Fay, S. D., Goodall, R., & Askes, H. (2016). Energy absorption in lattice structures in dynamics: Experiments. *International Journal of Impact Engineering, 89*, 49–61.

Bauer, J., Meza, L. R., Schaedler, T. A., Schwaiger, R., Zheng, X., & Valdevit, L. (2017). Nanolattices: an emerging class of mechanical metamaterials. *Advanced Materials, 29*(40), Article 1701850.

Pham, M. S., Liu, C., Todd, I., & Lertthanasarn, J. (2019). Damage-tolerant architected materials inspired by crystal microstructure. *Nature, 565*(7739), 305–311.

Maloney, K. J., Fink, K. D., Schaedler, T. A., Kolodziejska, J. A., Jacobsen, A. J., & Roper, C. S. (2012). Multifunctional heat exchangers derived from three-dimensional micro-lattice structures. *International Journal of Heat and Mass Transfer, 55*(9-10), 2486–2493.

Saleh, M. S., Li, J., Park, J., & Panat, R. (2018). 3D printed hierarchically-porous microlattice electrode materials for exceptionally high specific capacity and areal capacity lithium ion batteries. *Additive Manufacturing, 23*, 70–78.

Jiang, Y., Xu, Z., Huang, T., Liu, Y., Guo, F., Xi, J., & Gao, C. (2018). Direct 3D printing of ultralight graphene oxide aerogel microlattices. *Advanced Functional Materials, 28*(16), Article 1707024.

Sun, H., Zhu, J., Baumann, D., Peng, L., Xu, Y., Shakir, I., & Duan, X. (2019). Hierarchical 3D electrodes for electrochemical energy storage. *Nature Reviews Materials, 4*(1), 45–60.

Milton, G. W., & Cherkaev, A. V. (1995). Which elasticity tensors are realizable? *Journal of Engineering Materials and Technology, 117*, 483–493.

Vasquez, F.G., Milton, G.W., Onofrei, D., Seppecher, P. (2013). Transformation elastodynamics and active exterior acoustic cloaking. In *Acoustic Metamaterials* (pp. 289-318). Springer, Dordrecht.

Bückmann, T., Kadic, M., Schittny, R., & Wegener, M. (2015). Mechanical cloak design by direct lattice transformation. *Proceedings of the National Academy of Sciences, 112*(16), 4930–4934.

Pasternak, E., & Dyskin, A. V. (2018). Rotational waves in layered solids with many sliding layers. *International Journal of Engineering Science, 125*, 40–50.